# Defect Detection in LENS AM Using In Situ Thermal Camera Process Monitoring

**Tom Stockman, Judith Schneider, Cameron Knapp, Kevin Henderson and John Carpenter**

**Abstract** This study utilizes in situ thermal imaging to monitor the melt pool during a LENS additive manufacturing (AM) process. A software tool is created which gathers metrics for each frame and summarizes them over every build. Plotted metrics allow a user to visually inspect the data, but the software tool also automatically identifies anomalies and flags them for further review. Anomalies are then correlated to physical locations in the build which are inspected for defects. This type of process monitoring could lead to fast detection of defects during a build, thus increasing the confidence in production quality and eliminating the acceptance of parts with abnormalities. An anomalous event was identified by the software tool and investigated with X-ray computed tomography. Defects were observed in the location identified by the software tool.

**Keywords** Process monitoring · LENS · Additive manufacturing

## Introduction

AM is rapidly being integrated into production environments where parts must not only conform to specific geometrical tolerances but also perform structurally under significant stress and fatigue. Such a shift from prototyping to end-use products has increased demand for rigorous quality control [1]. The aerospace industry, for example, has begun adoption of AM parts into rocket engines where constant vibration makes fatigue a critical component to part performance. Such performance requirements mean that defects within the part can be detrimental. The term

T. Stockman (✉) · J. Schneider
University of Alabama in Huntsville, Huntsville, USA
e-mail: tom.j.stockman@gmail.com

J. Schneider
e-mail: jas0094@uah.edu

C. Knapp · K. Henderson · J. Carpenter
Los Alamos National Laboratory, Los Alamos, USA



The Minerals, Metals & Materials Society, *TMS 2018 147th Annual Meeting & Exhibition Supplemental Proceedings*, The Minerals, Metals & Materials Series,
https://doi.org/10.1007/978-3-319-72526-0_10

"defect" refers to a wide range of features that can be used to describe an anomaly in a build which would likely reduce its structural performance. Such defects could include, but are not limited to, lack of fusion, delamination, surface roughness, and unusually large or misshapen porosity [2]. This study focuses on Laser Engineered Net Shaping (LENS) which is a freeform AM process in which metallic powder is blown through nozzles into the path of a laser forming a melt pool.

In this study, the process is monitored using a camera with a two-color pyrometer to detect changes in the melt pool temperature profile during a build. As the metal is deposited onto a build plate, the camera records the temperature distribution within the melt pool region. Each frame from the camera is analyzed looking for anomalous behavior which is correlated to a location in the build. That location is then scanned using X-ray Computed Tomography (XCT) to investigate the abnormality.

Uses of high speed cameras, with framerates on the order of 5000 Hz, have been reported for in-situ process monitoring of AM processes [3, 4]. This study, however, uses a very low framerate (9.310 Hz) in an attempt to explore solutions which would be more readily accepted into a production environment. This lower framerate allows rapid processing of the data and extraction of a wide range of features from each frame without significant computational burden. By correlating the data obtained with defects in actual parts, the combination of metrics gathered from each frame can be identified as signatures of particular defect type. Although it is possible to miss defects with signatures on a timescale or length scale small enough to fit between frames. Continued in-situ and ex-situ analysis are needed to determine the false positive and false negative rates of any software tool developed.

## Experimentation

The LENS machine used in this study was an Optomec LENS MR-7 [5] which is a blown powder system with 3 axis control housed within a glovebox as shown in Fig. 1. The base moves in X and Y while the deposition head moves in Z. The MR-7 is equipped with a 1 kW IPG fiber laser in an enclosed argon atmosphere (<10 ppm $O_2$). Several diagnostic tools have been installed in the machine, including a ThermalViz camera system used in this study. The camera uses a two-color pyrometer with 950 and <950 nm wavelengths, overlaying two discreet sensors to correct for emissivity. A tungsten filament is used to calibrate the temperature measurements with a linear temperature-radiance ratio. The data was sampled at 9.310 Hz, the maximum rate of the camera, with an exposure time of 20 ms. The pyrometer looks directly down onto the build plate coaxial with the laser.

The power delivered from the MR-7 LENS laser was 808 W focused at a distance of 0.9525 cm and with a powder feed rate of 33.7 g/min. Powders used were 304L with an average size of 100 μm. The dwell time for the laser starting each pass was 20 ms, and the travel speed of the table was 101.6 cm/min. The length of each pass was 5.08 cm with a 0.102 cm hatch spacing for the second pass

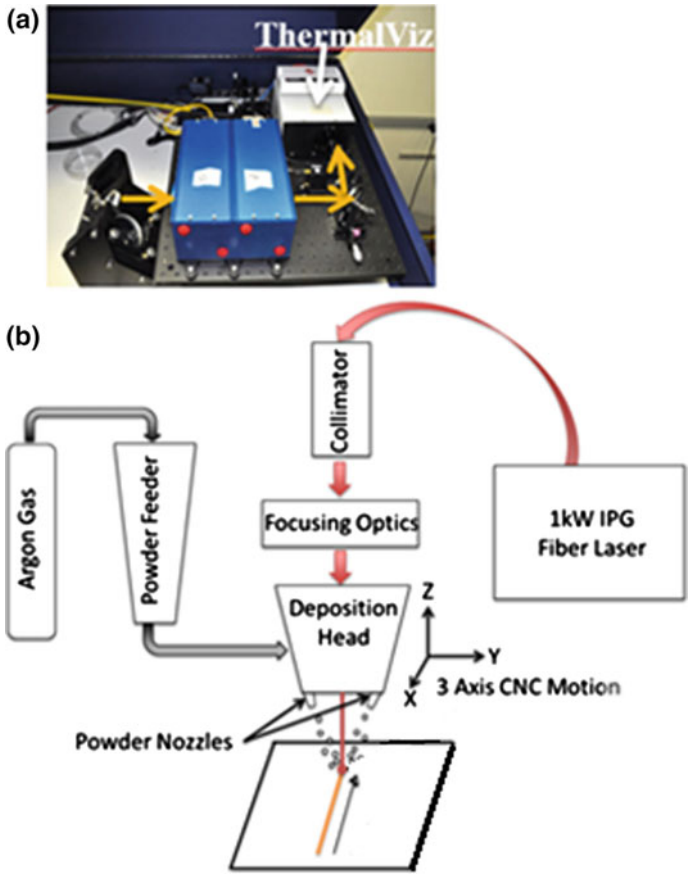


**Fig. 1** **a** Shows the ThermalViz pyrometer looking down coaxial with the laser. **b** Shows the MR-7 schematic

deposited next to the first as illustrated in Fig. 2. Parameters were selected to create a fully dense deposit with no effort made to 'insert' a known population of defects. The print geometry used in this study was 5.08 cm long by 0.102 cm wide and 0.076 cm high.

## In Situ Analysis

ThermalViz software was used to convert the data files from the camera into comma separated value (CSV) format. A custom Python script was used to process the CSVs. For each frame, a "summary image" is generated which compiles four different views of the data as shown in Fig. 3: (a) a colorized heat map, (b) the melt pool isolated with several features drawn on top of it, (c) a contoured heat map, and

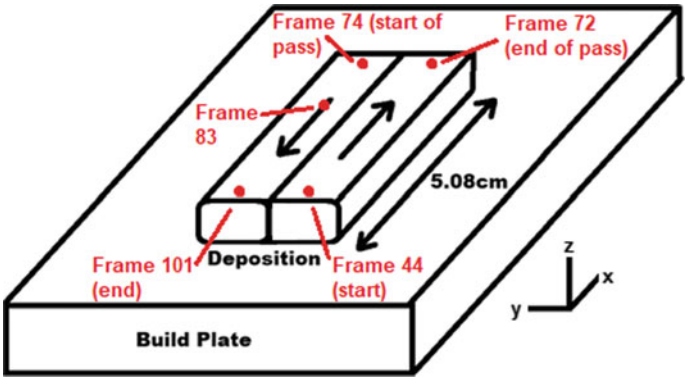


**Fig. 2** Deposition plan used, 5.08 cm long, 2 layers deposited in alternating directions spaced 0.1016 cm apart

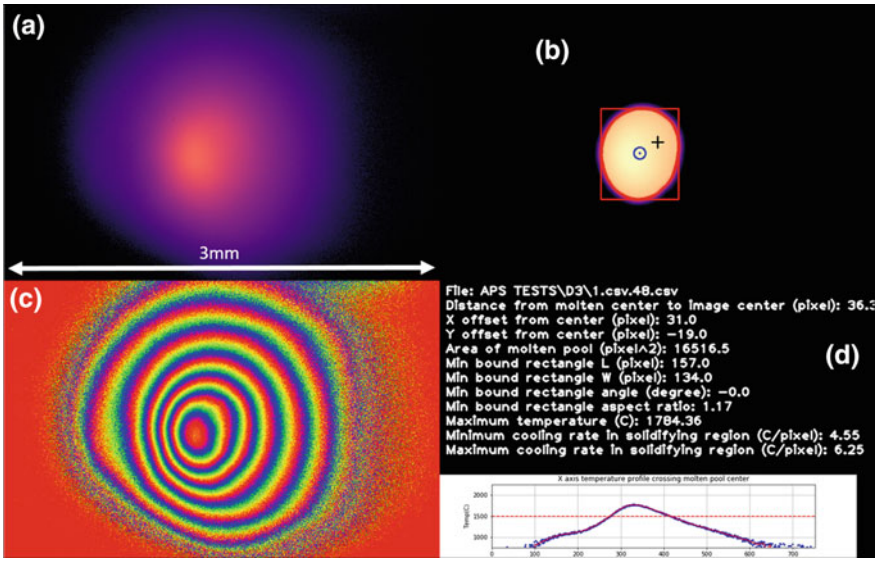


**Fig. 3** A typical "Summary Image". **a** heat map, **b** molten pool, **c** contoured heat map, **d** frame metrics. The scale shown in (**a**) is the same for (**b**) and (**c**)

(d) a listing of several metrics recorded from that frame with an X direction plot of the temperature profile through the center of the melt pool (the blue circle in (b)) (Fig. 3). The contours are interpreted using the "prism" scale shown in Fig. 4.

The melt pool is generated by thresholding the original image to only pixels above a certain temperature value. In this case 1500 °C was chosen as the threshold temperature. This is slightly above the 1340 °C melting temperature of 304L which was chosen to ensure the identified region was molten. It is worth noting that the


**Fig. 4** Matplotlib color map "prism" set to repeat approximately every 150 °C. The maximum temperature recorded in Fig. 3c was 1784 °C and can be seen visually by the number of repeating color bands across the contours to the final red color in the center of the molten pool

collection of these metrics from the melt pool region are not necessarily meant to be physically significant. The purpose of the analysis is to spatially resolve the location of anomalies and outliers; thus only consistency is required.

Once thresholded, the molten pool area is blurred. Unlike the colorized contour plot, a blur is required so that the software can draw a defined solid line around the region of interest. From the blurred molten pool the following metrics are gathered: center of mass, area, minimum bounding rectangle. These metrics are determined using the python library OpenCV and are summarized in Table 1.

**Table 1** Metrics gathered from each frame with a brief description, typical measured values, and anomalous frame values

| Metric | Description | Mean | St Dev | Frame 83 | Difference from 83 to mean (%) |
|---|---|---|---|---|---|
| Distance (pixels) | Distance from molten pool CoM to pixel center of image | 26.10 | 8.36 | 21.47 | −17.80 |
| X offset (pixels) | X direction component of distance | 20.68 | 9.76 | 19.00 | −8.10 |
| Y offset (pixels) | Y direction component of distance | −13.98 | 6.36 | −10.00 | −28.50 |
| Area (pixels$^2$) | Sum of molten pixel areas | *16767.41* | *3644.96* | *3587.00* | *−78.60* |
| Length (pixels) | Length of smallest bounding rectangle around molten pool | *166.96* | *16.69* | *107.35* | *−35.70* |
| Width (pixels) | Width of smallest bounding rectangle around molten pool | *126.66* | *19.28* | *48.66* | *−61.60* |
| Aspect ratio (Length/Width) | Length/Width parameters specified above | *1.34* | *0.19* | *2.21* | *64.70* |
| Max Temp (°C) | Maximum temperature in image | *1717.03* | *78.74* | *1540.18* | *−10.30* |
| Heating Rate (°C/pixel) | Temperature rate of change on leading edge of molten pool | *4.04* | *0.76* | *1.67* | *−58.70* |
| Cooling Rate (°C/pixel) | Temperature rate of change on trailing edge of molten pool | *5.84* | *1.43* | *2.08* | *−64.40* |

Two metrics are gathered from the area just outside the molten pool which are called the "Heating Rate" and "Cooling Rate". These are created by thresholding the original image to isolate pixels in the temperature range of 1450–1500 °C. The range of 50 °C was selected to be broad enough to be significant, but narrow enough that temperature profile in this range would be linear. This 50 °C band around the melt pool is blurred so that contours can be drawn, and the thickness of the contour measured on both the leading and trailing edge of the molten pool. The pixel thickness of each is then divided by the temperature span of 50 °C to get a cooling rate in °C/pixel. This can later be converted to °C/m using the actual length of the image pixels and then into °C/s using the m/s table travel speed. An algorithm was developed to determine the direction of travel which was used to differentiate the "Heating Rate" from the "Cooling Rate".

In this study potential defects are identified by searching for statistical anomalies in the recorded metrics. After metrics are gathered for each frame, they are plotted and outliers are identified. For this initial study, anomalies are identified relative only to the data set of the current build. For each metric summarized in Table 1, the data is first analyzed while looking for data points which are more than four standard deviations from the mean. The frame location of these outliers is recorded, and those data points are removed from the data set. After the removal of extremes, the mean and standard deviations are recalculated, and any data points outside two standard deviations are also recorded. If a frame is identified as an outlier in more than three metrics, it is automatically flagged as an anomaly. Frames which are flagged as anomalies are then correlated to a location in the build so that XCT scans can be performed to look for defects. Figure 5 shows an example plot of the processed data with lines drawn to show one and two standard deviations away from the mean. Similar plots were generated for every metric gathered.

To guide the XCT scans, the location of the captured frame to a location in the build must be identified. However the LENS machine does not timestamp the frames thus there is no time/position data recorded. To provide this correlation, a combination of build path parameters and signatures in the thermal data are used to make an appropriate correlation. The passes in each build alternate in the negative and positive X directions as illustrated in Fig. 2. There is a brief pause between these passes while the machine adjusts in the Y direction. The pause is long enough to generate several dark frames in the data. Thus whenever two to three frames are missing this marks the beginning of a new pass which is assigned a pass number. To determine the position of the frame within that pass, a camera framerate of 9.310 Hz is used. Thus by counting the number of frames from the start of the pass, and knowing the travel speed of the table, the distance traveled can be calculated.

Because the time since the start of a pass is being used to calculate the position, any uncertainty in the time also propagates into the position. Two sources of uncertainty were quantified. First there is a uniformly distributed uncertainty about the start time of the build. Although the time associated with the laser on is unknown, it occurs sometime between the first frame where it is visible and the frame immediately prior. This uncertainty will be present regardless of the framerate of the camera, but the associated uncertainty scales inversely with the

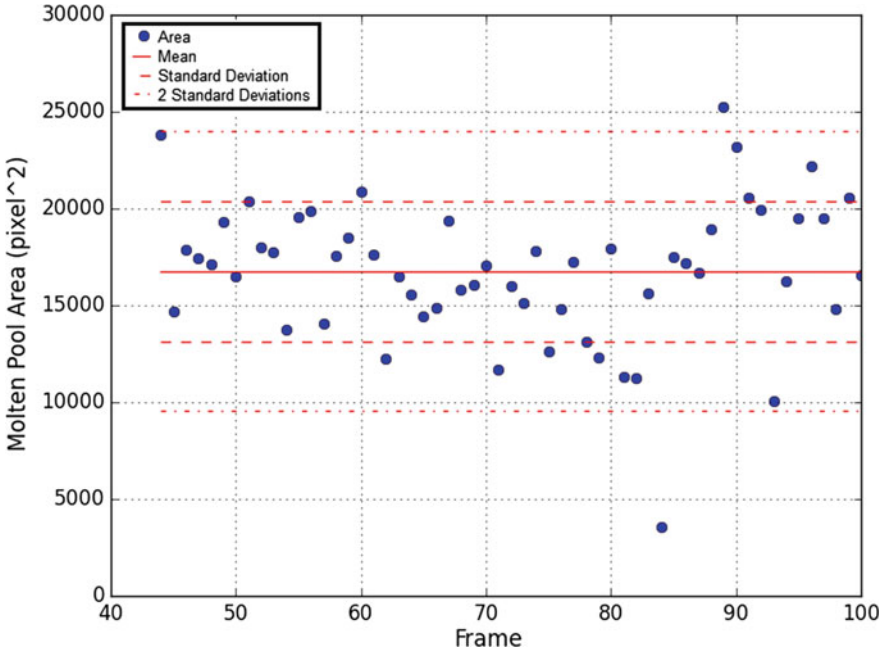


**Fig. 5** Molten pool area (pixels$^2$) in each frame. Note that frame 83 falls outside of the standard deviation range. Frame 48 (marked by an arrow) represents the average frame used for comparison of melt pool size in Fig. 7

framerate. The second source of uncertainty is on the framerate itself. ThermalViz reports the framerate at the end of a build as an average of the number of frames taken over the total time it was running, but there is no information available on the consistency of that framerate. A normal distribution with a 1% standard deviation was assumed for the time between each frame meaning that this component of the uncertainty grows with each consecutive frame after a new pass has begun. This growth is modeled by a normal distribution about the sum of its constituent means and with a variance equal to the sum of its constituent distribution variances [6]. However because the position of the start of each pass is known from the coding input to the LENS machine, the growing component of the uncertainty can be reset to 0 at the start of each pass, hence referred to as a baseline event. Figure 6 plots the sum of these two uncertainties converted from time uncertainty to position uncertainty by multiplying by the travel speed. The travel speed is assumed constant with expected uncertainty of less than 1%. The three lines show three different confidence levels which were considered when identifying the location of particular frames.

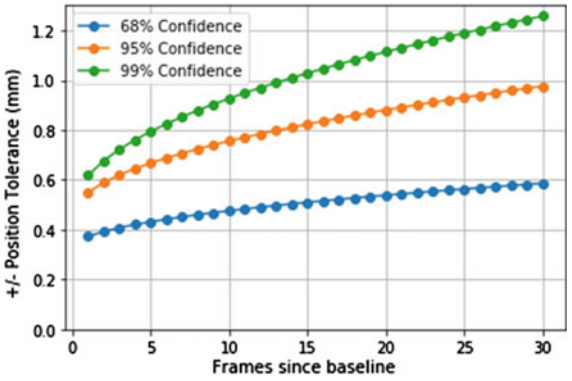


**Fig. 6** Quantified positional uncertainty in the X direction at three confidence levels. Frame 83 from Fig. 5 is 10 frames since baseline. The position of this frame is known to within ±0.75 mm with a 95% confidence

## Anomaly Detection Results

The analysis method used in this study identified two frames as anomalous: Frames 44 and 83. Frame 44 was omitted from further investigation as the camera is turned on for some time before the build actually begins, and the 44th frame from the camera initialization is the start of the build. The reason this frame flagged as unusual is that unlike subsequent frames, the current frame was symmetrical because the base plate had not yet begun to move. This made the shape, area, and position of the melt pool flag as outliers in the analysis. Thus it is not recommend to use the first frame of a build for outlier analysis.

Figure 7 shows the melt pools from summary image of Frame 83 which was considered for further analysis and Frame 48 which is representative of the rest. Frame 83 was flagged as an outlier in seven metrics: area, length, width, aspect ratio, maximum temperature, heating rate, and cooling rate. Table 1 shows some quantification of the metrics averaged over the whole build along with the specific values of frame 83. Frames which flagged as outliers are italicized. A typical frame

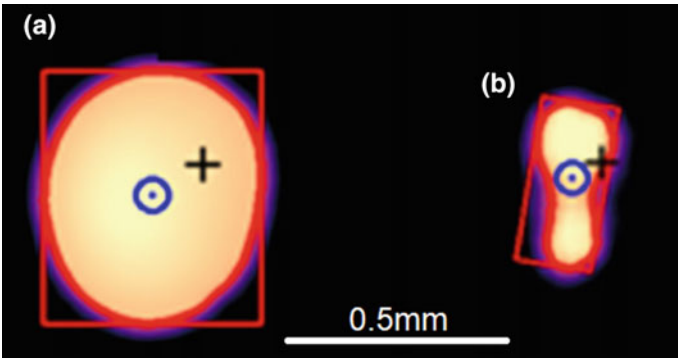


**Fig. 7** Melt pools for **a** a normal frame (as seen in Fig. 3) and **b** Frame 83

is shown in Fig. 7a in contrast with frame 83 shown in Fig. 7b. The molten pool is visibly smaller and misshapen. Thus type of fluctuation could be due to anomalies in powder flow or laser power. Changes in these critical parameters could cause defects.

## Ex-Situ Measurement

After the build was completed, it was inspected using an Xradia Micro Computed Tomography (XCT) machine. The X-ray source was a Micro Focus Hamamatsu operated at 40–150 kV acceleration voltage, 10 W total power, and 5 μm spot. The detector was a 2048 × 2048 pixel camera coupled with a scintillator crystal lens. The voxel dimension was 5 μm corresponding to a detectable defect size. The TXMReconstructor software package (Carl Zeiss Microscopy, Inc.) was utilized for tomogram reconstructions.

Figure 8 shows a lower density region or defect located near the identified area for Frame 83 but outside of expected location uncertainty bounds. The image shown is in the pass directly next to the location corresponding to Frame 83. Further testing of the part is needed to determine if the abnormality detected affects the structural property of the component.

## Future Work

This study is on-going to identify abnormalities in the melt pool during a build. Initially the data obtained will be evaluated with respect to an individual build. The ability of the analysis tool developed demonstrated the ability to measure and calculate several metrics from the acquired frames. The metrics were used to

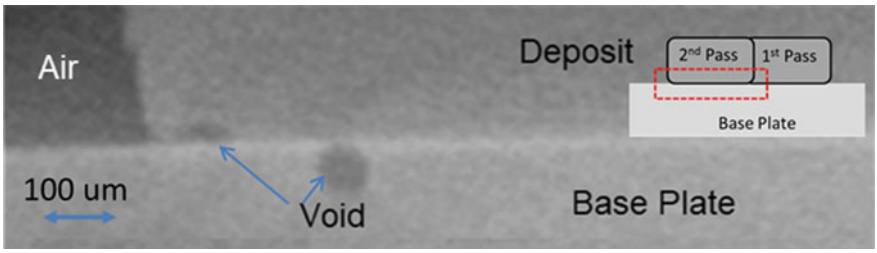


**Fig. 8** Density difference observed in XCT scan in area near location identified as Frame 83. Dark gray areas marked as 'voids' indicate where density is lower than expected. The very dark area to the top left is open air not inside the material. Both voids are ~100 μm in diameter and, when summed, are 40% of the normal melt pool diameter seen in Fig. 7

identify anomalous behavior in a particular frame which can be correlated to a specific location in the build.

As the database of abnormalities are continued to be collected and correlated with impact on material properties this will provide a training dataset for subsequent analysis. Using this training set, more sophisticated methods can be developed to identify critical signatures in the data. Narrowing the required number of metrics would allow for faster processing thereby facilitating real time analysis. If an abnormality can be detected, the build can be terminated to reduce time in obtaining an acceptable quality build.

This type of data processing would benefit from AM equipment equipped with a time stamp. Although extrapolation of the position from the number of frames is possible, accuracy would be improved by having a timestamp directly correlated to a position within the build.

## References

1. NIS (2013) Measurement science roadmap for metal-based additive manufacturing. Energetics Incorporated
2. Frazier WE (2014) Metal additive manufacturing: a review. J Mater Eng Perform 23(6): 1917–1928
3. Berumen S, Bechmann F, Linder S, Kruth J-P, Craeghs T (2010) Quality control of laser and powder bed-based additive manufacturing (AM) technologies. Phys Procedia 5:617–622
4. Furumoto T, Ueda T, Alkahari MR, Hosokawa A (2013) Investigation of laser consolidation process for metal powder by two-color pyrometer and high-speed cideo camera. CIRP Ann Manuf Technol 62(1):223–226
5. Optomec. www.optomec.com/wp-content/uploads/2014/04/LENS_MR-7_Datasheet_WEB_0816.pdf. Accessed 10 Sept 2017
6. Eisenburg B, Sullivan R (2008) Why the sum of independent normal random variables is normal. Math Mag 81:362–366